CHALMERS
UNIVERSITY OF TECHNOLOGY

Divergent Responses of Multi-frequency Vegetation Optical Depth Products to Climate Variations in China

Journal of Remote Sensing
A SCIENCE PARTNER JOURNAL

RESEARCH ARTICLE

Divergent Responses of Multi-frequency Vegetation Optical Depth Products to Climate Variations in China

Mingzhu He[1,2], Yonghong Yi[3*], Xiaojun Li[4], Jean-Pierre Wigneron[4], John S. Kimball[5], Rolf Reichle[6], Lei Fan[7], and Hans W. Chen[8]

[1]Joint International Research Laboratory of Catastrophe Simulation and Systemic Risk Governance, Beijing Normal University, Zhuhai 519087, China. [2]School of National Safety and Emergency Management, Beijing Normal University, Zhuhai 519807, China. [3]College of Surveying and Geo-Informatics, Tongji University, Shanghai, China. [4]INRAE, UMR1391 ISPA, Université de Bordeaux, F-33140 Villenave d'Ornon, France. [5]Numerical Terradynamic Simulation Group (NTSG), W.A. Franke College of Forestry and Conservation, University of Montana, Missoula, MT, USA. [6]Global Modeling and Assimilation Office, NASA Goddard Space Flight Center, Greenbelt, MD, USA. [7]Chongqing Jinfo Mountain Karst Ecosystem National Observation and Research Station, School of Geographical Sciences, Southwest University, Chongqing, China. [8]Department of Space, Earth and Environment, Chalmers University of Technology, Gothenburg, Sweden.

*Address correspondence to: yonghong_yi@tongji.edu.cn

Citation: He M, Yi Y, Li X, Wigneron J-P, Kimball JS, Reichle R, Fan L, Chen HW. Divergent Responses of Multi-frequency Vegetation Optical Depth Products to Climate Variations in China. *J. Remote Sens.* 2026;6:Article 1028. https://doi.org/10.34133/remotesensing.1028

Submitted 17 February 2025
Revised 4 November 2025
Accepted 12 November 2025
Published 2 February 2026

Vegetation optical depth (VOD) has been widely assessed for satellite monitoring of vegetation carbon and water status under different environmental conditions. However, abilities of multi-frequency VODs to reflect the integrated dynamics in vegetation status under changing climate are still underinvestigated, especially in China, which has experienced substantial vegetation greening since 2000. To fill this gap, this study examines 7 VOD products for their capabilities to detect vegetation status changes under climate variations from 2012 to 2022 in China. We find divergent responses of multi-frequency VODs to climate variations in China, and the retrieval frequency is the most important factor, followed by the underlying retrieval algorithms. All 7 VOD products show stronger responses to water limitations (atmospheric and soil water stress) than temperature across different plant functional types in China, suggesting high potential of VOD to track vegetation water status changes. We also find that the capabilities of VODs to represent vegetation responses to climate variations are affected by vegetation growth limitations, showing consistent responses for ecosystems dominated by either temperature or water. Most importantly, we find that VODs capture well the carry-over effects of climate on vegetation dynamics in China, with X- and C-band VODs showing stronger abilities than L-band VODs, especially for ecosystems located in China's arid and semiarid regions. These findings address the divergent capabilities of multi-frequency VOD products to capture the vegetation responses to climate variations across China, promoting ecological applications of different VOD products in regional studies.

Introduction

Vegetation optical depth (VOD) parameterizes the extinction of microwave emissions by the vegetation canopy and has attracted wide attention in recent years. Unlike optical-infrared remote sensing-based vegetation indices, microwave-based VOD retrievals are sensitive to changes in vegetation water content and generally less affected by solar illumination and atmospheric effects, and thus increasingly used for monitoring vegetation dynamics associated with changes in aboveground biomass or water content [1–4].

Studies have shown that VOD products derived from different frequencies and algorithms convey different information in terms of vegetation carbon and water dynamics [5]. VOD retrieved from relatively high frequencies have been reported to have good performance for representing vegetation canopy changes. For example, 10.7 GHz (X-band) VOD constructed from an established Land Parameter Data Record (LPDR) algorithm using data from both the Advanced Microwave Scanning Radiometer for EOS (AMSR-E) and Advanced Microwave Scanning Radiometer 2 (AMSR2) showed potential for quantifying the global impact of El Niño–Southern Oscillation events on vegetation health [6]. Moreover, AMSR-E/AMSR2 LPDR X-band VOD was sensitive to aboveground biomass (AGB) variations in the contiguous USA [7] and drought-driven tree mortality in California, USA [8].

VOD products from higher frequencies (i.e., X-band) are found to be more sensitive to biomass dynamics from the upper

canopy and under low to moderate AGB than those derived from lower frequencies, while approaching signal saturation for deep canopy layers and dense AGB cover. In comparisons, VODs retrieved from relatively low frequencies, such as L-band (1.4 GHz), show advantages in capturing AGB variations from a larger forest canopy volume [1,5,9–11]. For example, L-band VOD has shown high potential to characterize the interannual AGB dynamics at continental and global scales [12–15], and may be suitable to produce global maps of annual live vegetation biomass [16]. However, high temporal correlations among X-, C-, and L-band VODs may exist in ecosystems with low biomass. Furthermore, VODs from multiple frequencies, such as Ku-, X-, C-, and L-band, were applied to estimate gross primary production globally, providing additional information about vegetation photosynthesis beyond optical data and aiding carbon source and sink estimations across different ecosystems [16–18].

Besides the ability to monitor terrestrial carbon dynamics, VOD products from multiple frequencies also show high sensitivity to vegetation water content changes. Ku-, X-, and C-band VODs from the VODCA (Vegetation Optical Depth Climate Archive; [19]) dataset, a merged global long-term VOD product retrieved from multiple sensors, have been used to estimate leaf moisture content globally, suggesting possible VOD applications for assessing large-scale spatial and temporal changes in vegetation water status, drought conditions, and wildfire dynamics [2]. SMAP (Soil Moisture Active Passive) L-band VOD was successfully used as a plant water proxy to identify vegetation water stress from surface drying and heating across diverse biomes in Africa [20]. In particular, due to its close relationship with vegetation water content, VOD could be used to estimate plant stomatal regulation strategies [21–23], and has been used to investigate the water stress impacts on grassland productivity due to excessive vapor pressure deficits (VPDs) [21].

The capability of VOD from different algorithms, frequencies, and sensors to detect vegetation changes may vary spatially and temporally across different plant functional types (PFTs). A recent study by Konings et al. [24] reported that VOD may vary differently from year to year for many PFTs, highlighting the importance of clarifying the capability of VOD products across different vegetation types. Global assessments of several VOD products showed that the global relationships between VOD and vegetation properties are complex and may differ with land cover types [5,25], highlighting the necessity of selecting the most suitable product for representing vegetation dynamics at regional to global scales.

Although assessments of multiple VOD products have been conducted globally or regionally, the VOD capability to capture vegetation dynamics under climate variations for different ecosystems in China is still unclear. China has experienced substantial greening since 2000 [26,27], mainly due to ecological engineering programs to conserve and expand forests [28]. In order to achieve the goals of carbon peaking in 2030 and carbon neutrality in 2060, it is important to understand how vegetation responds to climate variations and may act to reinforce or mitigate future climate change. As optical-infrared remote sensing-based vegetation indices may be contaminated by various atmospheric conditions (e.g. clouds), VOD has distinct advantages for representing the integrated vegetation dynamics in terms of both carbon and water content changes under a changing climate, raising the need for comprehensive evaluations of different VOD products in China.

In this study, we aim to evaluate the capability of multiple VOD products from available satellite records involving different microwave frequencies (X-, C-, and L-band), several sensors (AMSR-E, AMSR2, SMAP, and Soil Moisture and Ocean Salinity [SMOS]), and different retrieval algorithms to indicate the integrated vegetation responses to climate variations in China from 2012 to 2022. The vegetation variations responding to air temperature (Ta), atmospheric VPD, and soil moisture (SM) changes are evaluated spatially and temporally during the study period. The carry-over (or legacy) effects of climate variables on vegetation dynamics represented by the different VOD products across different PFTs are discussed. Finally, the impacts of the different retrieval algorithms and frequencies on VOD applications are addressed to advance our understanding of VOD responses to climate in China.

Materials and Methods

Study domain

In this study, we use a 1:1,000,000 digitized vegetation map to depict vegetation distributions in China, which is provided by the Environmental & Ecological Science Data Center for West China, National Natural Science Foundation of China (https://www.resdc.cn/data.aspx?DATAID=122). Seven major PFTs are analyzed here, including temperate forests (TF), subtropical forests (SF), temperate non-forests (TNF), alpine grassland (AG), and cropland, which is separated into 3 classes according to planting and harvesting habits: cropland with 1 or 2 harvests per year (CRO1 and CRO2, respectively) and cropland with 3 harvests over 1 or 2 years (CRO3). TNF mainly includes temperate grassland and shrubs, and is mostly distributed from the northeast to northwest parts of China (Fig. 1) and is generally limited by water availability (Fig. S1B). TNF accounts for about 26.9% of the total vegetated areas in China, and has the largest coverage among all 7 examined PFTs. SF is mainly located in the southern part of the study domain, and accounts for about 19.5% of the total vegetated areas. AG covers about 19.3% of the study domain, and is mainly distributed in the Qinghai-Tibetan Plateau region. Cropland accounts for 24.0% of the total vegetated area in China, with CRO1, CRO2, and CRO3 covering about 7.2%, 7.6%, and 9.2% of the total land area, respectively.

Data

In this study, we use freely available VOD products retrieved from low (L-band) to high (X- and C-band) frequencies available from AMSR-E/AMSR2, SMAP, and SMOS sensors from 2012 to 2022 (Table 1). Since SMAP was launched in 2015, SMAP-based VOD products were examined over the period from 2015 to 2022.

The X-band VOD product from the AMSR Land Parameter Data Record (LPDR-X) version 3 was derived from calibrated AMSR-E and AMSR2 observations. Such VOD was generated from an iterative multi-frequency brightness temperature retrieval algorithm by inverting the frequency-based land–water microwave emissivity slope index [29,30], where VOD was derived simultaneously with surface temperature and fractional water cover as a prerequisite for SM retrieval under ice-free conditions. The algorithm incorporated a temporal smoothing filter (60 days) to remove the high-frequency fluctuations [29].

This study used 3 VOD products derived from the Land Parameter Retrieval Model (LPRM) using the AMSR2 record [31,32], including C1-band (6.9 GHz; LPRM-C1), C2-band (7.3 GHz; LPRM-C2), and X-band (10.7 GHz; LPRM-X). The

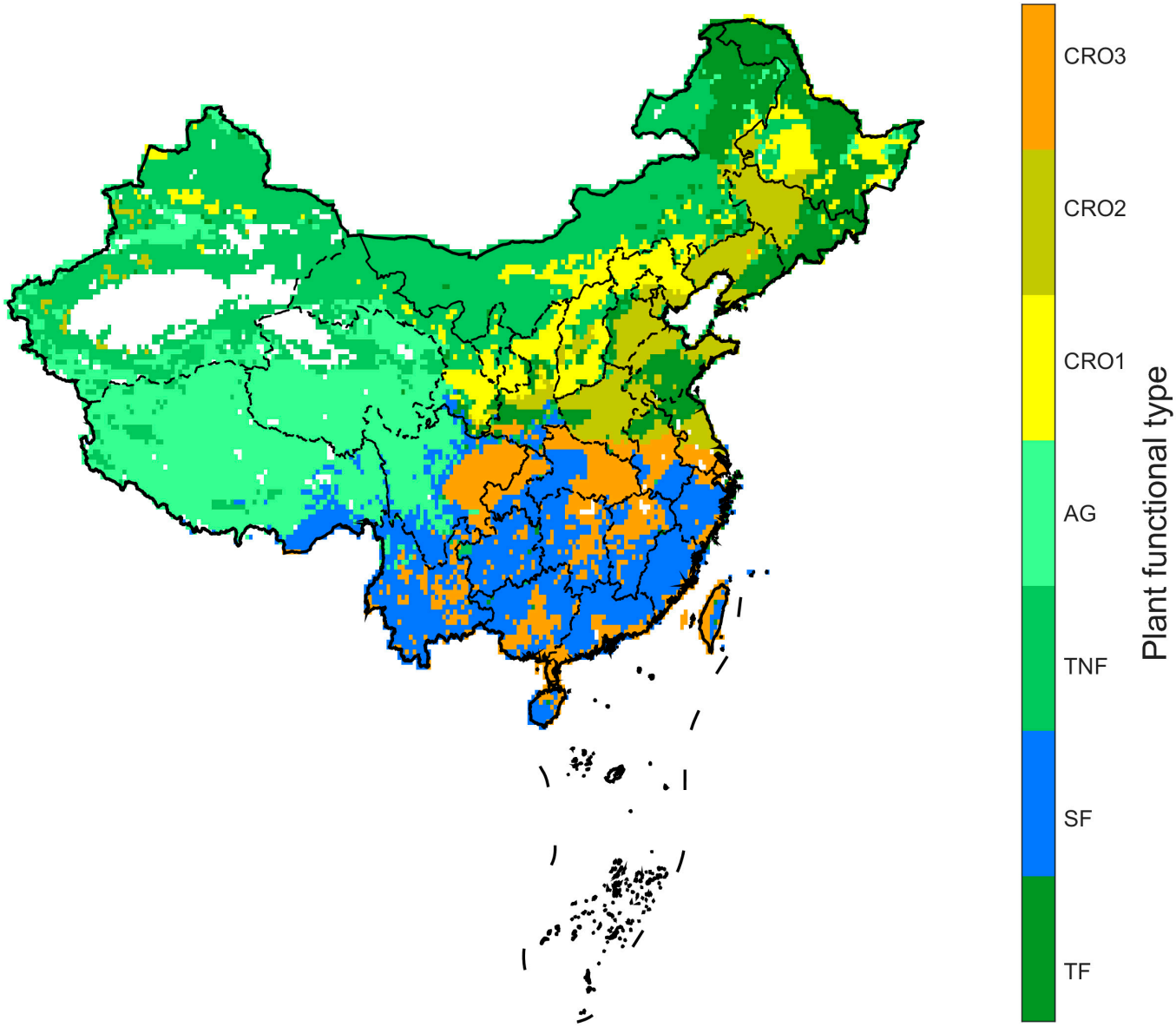

Fig. 1. The spatial distributions of vegetation types in China adapted from a 1:1,000,000 digitized vegetation map (https://www.resdc.cn/data.aspx?DATAID=122). The major vegetation types in China include temperate forests (TF), subtropical forests (SF), temperate non-forests (TNF), alpine grassland (AG), cropland of 1 harvest per year (CRO1), cropland of 2 harvests per year (CRO2), and cropland of 3 harvests over 1 or 2 years (CRO3).

Table 1. The characteristics of VOD products used in this study

VOD product	Sensor	Frequency	Algorithm	Resolution	Time period	Reference
LPDR-X	AMSR-E, AMSR2	10.7 GHz	LPDR	Daily, 25 km	2012–2022	Du and Kimball [30]
LPRM-X	AMSR2	10.7 GHz	LPRM V5	Daily, 25 km	2012–2022	Owe et al. [32]
LPRM-C2	AMSR2	7.3 GHz	LPRM V5	Daily, 25 km	2012–2022	Owe et al. [32]
LPRM-C1	AMSR2	6.9 GHz	LPRM V5	Daily, 25 km	2012–2022	Owe et al. [32]
SMAP-DCA	SMAP	1.4 GHz	DCA	Daily, 9 km	2015–2022	O'Neill et al. [34]
MCCA-SMAP	SMAP	1.4 GHz	MCCA	Daily, 9 km	2015–2022	Peng et al. [38]
SMOSMAP-IB	SMAP, SMOS	1.4 GHz	SMOS-IC	Daily, 36 km	2012–2022	Li et al. [36]

LPRM algorithm is based on a forward radiative transfer model to retrieve VOD and can be applied at any microwave frequency [32]. Both horizontal and vertical polarization brightness temperature are used without using any auxiliary data on vegetation properties to generate VOD product. Specifically, we used the daily 25-km LPRM-C1, LPRM-C2, and LPRM-X VOD products from 2012 to 2022.

Three L-band VOD products were also included in this study, including the SMAP operational L3SM product based on a dual-channel algorithm (SMAP-DCA; [33,34]), L-band VOD derived from the multichannel collaborative algorithm using SMAP brightness temperature (MCCA-SMAP; [3,35]), and L-band VOD generated by fusing SMOS and SMAP data (SMOSMAP-IB; [36]). The SMAP dual-channel algorithm used brightness temperatures of both H and V polarization channels through a nonlinear least-squares minimization process to retrieve SMAP-DCA VOD at a 9-km spatial resolution [34]. MCCA-SMAP VOD was retrieved based on a self-constraint relationship between land parameters and an analytical relationship between brightness temperature at different channels. It is worth noting that the retrieval algorithms of MCCA-SMAP and SMOSMAP do not depend on any auxiliary data on vegetation properties and can be applied to a variety of satellites [37]. Daily 9-km MCCA-SMAP L-band VOD products [38] from 2015 to 2022 were used here. SMOS and SMAP are the 2 L-band radiometers currently in orbit, providing retrievals for SM and VOD at relatively low frequencies. Fusing SMOS and SMAP observations could potentially increase the number of observations used for VOD and SM retrievals. Thus, the SMOSMAP-IB algorithm combined the SMOS brightness temperature at a fixed incidence angle of 40° with the SMAP brightness temperature by using a monthly linear rescaling to generate a merged SMOS/SMAP brightness temperature data record; VOD was then retrieved through a mono-angular retrieval algorithm sharing a similar forward model with the SMOS-IC products [36]. Daily 36-km SMOSMAP-IB VOD products from 2012 to 2022 were used in this study.

In addition, as SM and VOD from the same product are generated simultaneously, they may be highly correlated with each other. Therefore, the ERA5-Land monthly SM dataset at the top soil layer (0 to 7 cm) with a spatial resolution of ~0.1° was provided by the European Centre for Medium-Range Weather Forecasts (ECMWF) [39], and served as an independent SM reference to characterize the impacts of soil water stress on vegetation. In comparison, the surface SM retrievals corresponding to each VOD product, including X-, C-, and L-band, were also included in this study to clarify the impacts of different retrieval algorithms and frequencies on VOD responses to SM. Meteorological data from the University of East Anglia Climate Research Unit (CRU; [40]), including Ta, and relative humidity (RH) at a spatial resolution of 0.5° and a monthly time step, were used here to analyze VOD variations under different climate conditions. VPD was then calculated using CRU-based Ta and RH, serving as an indicator of atmospheric dryness. To compare microwave-derived VOD with an optical, remote-sensing based vegetation index, the 500-m, 16-day Moderate Resolution Imaging Spectroradiometer (MODIS) Normalized Difference Vegetation Index (NDVI) product (MOD12Q1; [41]) from 2012 to 2022 was included in the analysis.

Methods

This study focuses on VOD retrievals to represent vegetation responses to climate variations in China during the 11-year period from 2012 to 2022, whereas SMAP-DCA and MCCA-SMAP VOD products are investigated from 2015 to 2022 since SMAP was launched in 2015. Here, we focus the analyses on growing season, defined as April to September, when most vegetation in China is active during this period. Additionally, by focusing on the growing season, we also avoid potential errors in VOD retrievals caused by frozen soil, which can complicate the interpretation of the results [19]. All 7 VOD products and the ancillary data are averaged monthly and resampled through the nearest-neighbor interpolation method to 25 km over the study domain.

The anomaly of each VOD dataset relative to the monthly climatology of 2012 to 2022 (2015 to 2022 for SMAP-DCA and MCCA-SMAP VODs) is calculated to focus on the vegetation dynamics. Similarly, the anomalies of Ta, VPD, and SM are also computed to represent the climate variations in China during the study period. The spatial and temporal Pearson correlation coefficients between different VOD anomalies and climate variables are shown to identify the vegetation dynamics responding to climate variations in China. The Pearson correlations are estimated using the monthly data (a total of 66 months in 11 years, or 48 months in 8 years for SMAP-DCA and MCCA-SMAP VODs) to account for both interannual and seasonal vegetation dynamics under a varying climate. The results at 95% significance level ($P < 0.05$) are also grouped for each PFT (Fig. 1) to disentangle the VOD variations across different vegetation types during the study period.

Based on the findings from a previous study indicating that high SM persistence can last up to 40 days [42], we repeated the analysis including a 1-month time lag to investigate the potential carry-over effects of climate variables (Ta, VPD, and SM) on VOD products. Specifically, we calculate the correlations between VOD anomalies and the anomalies in the 3 climate variables using data from both the previous and current months (a lag of 1 month) across different PFTs in China. For example, VOD anomalies in May are correlated with SM anomalies in April and May (1-month carry-over). Such correlations are then compared with the correlations calculated using anomalies from the same month to quantify the potential effects of climate variables carrying over from the previous month on the current month's vegetation status.

Results

Spatial variation of VOD at different frequencies across China

Generally, MODIS NDVI and all 7 VOD products show similar spatial patterns in China during the study period, with smaller values in the northwestern areas and larger values spanning from the northeastern to southern areas of China (Fig. 2). According to the land cover map (Fig. 1), TNF and AG typically have smaller NDVI and VOD, while forests (TF and SF) and croplands (CRO1, CRO2, and CRO3) show larger NDVI and VOD. Based on the same retrieval algorithm and sensors, as well as their close frequencies, the 3 LPRM-based VOD products share similar spatial variations and magnitudes across the study domain (Fig. 2C to E). Moreover, the spatial consistencies are found to be relatively high between the 2 X-band VODs ($r = 0.93$, $P < 0.05$) and the 2 C-band products ($r = 0.98$, $P < 0.05$). The 3 L-band VOD products (Fig. 2F to H) exhibit relatively large disparities in their spatial patterns for the same time period from 2015 to 2022 (r varies from 0.81 to 0.86, $P < 0.05$), indicating potential impacts

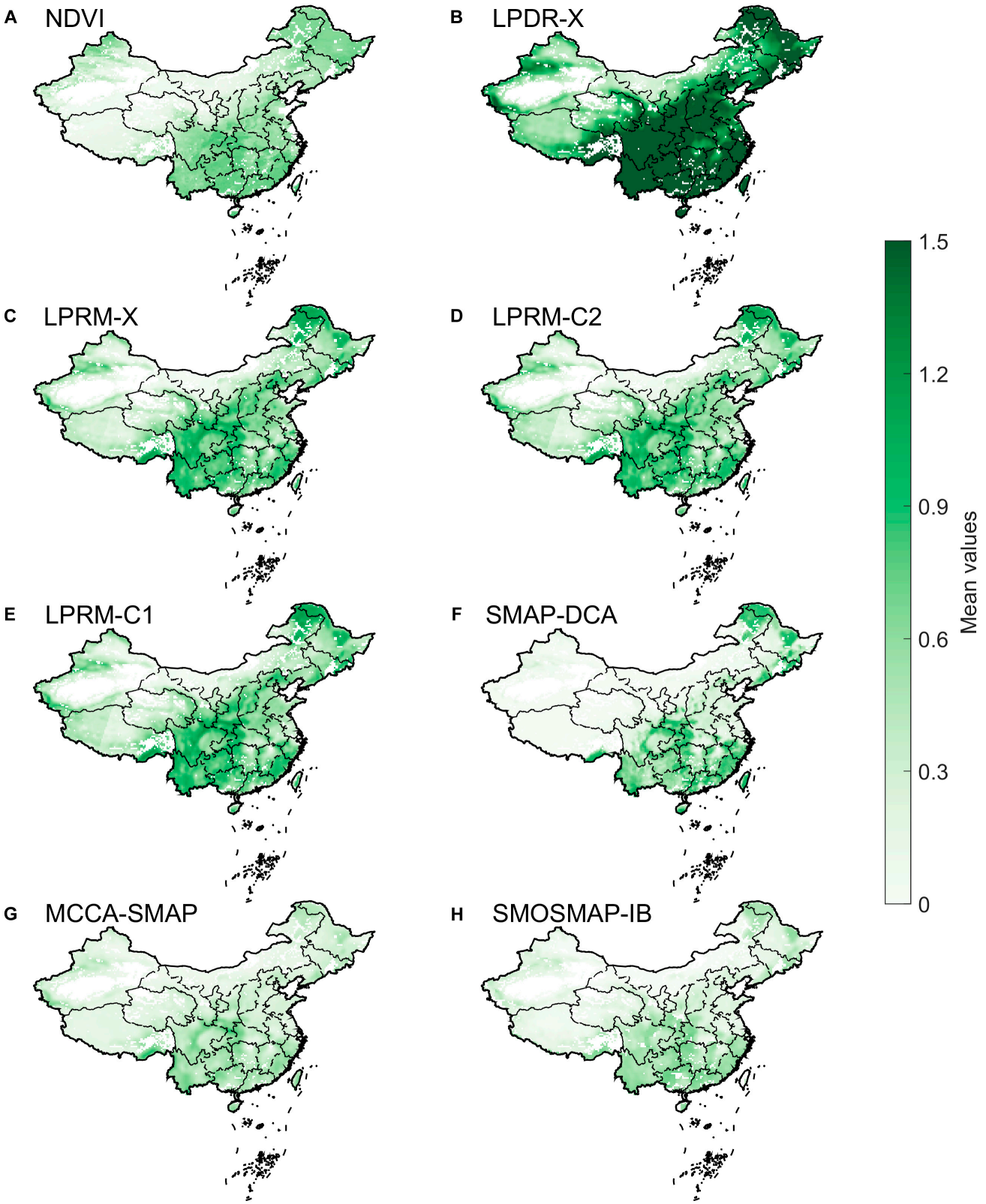

Fig. 2. Spatial distributions of mean growing-season NDVI and VODs in China averaged from 2012 to 2022. Mean growing-season MODIS NDVI is shown in (A). Different VOD products are shown, including VOD from AMSR-E/AMSR2 LPDR X-band (LPDR-X; B), AMSR2 LPRM X-band (LPRM-X; C), AMSR2 LPRM C2-band (LPRM-C2; D), AMSR2 LPRM C1-band (LPRM-C1; E), SMAP operational L-band DCA product (SMAP-DCA; F), MCCA-SMAP L-band (MCCA-SMAP; G) and SMOS/SMAP fused L-band VOD product (SMOSMAP-IB; H). Note that SMAP-DCA and MCCA-SMAP VODs are averaged from 2015 to 2022.

of different retrieval algorithms on the L-band VOD products. In summary, mean growing-season VOD values during the study period across China mainly vary with different PFTs and retrieval frequencies, with generally higher VOD values for forest ecosystems and at higher frequencies.

Spatially divergent VOD responses to climate variations in China

Here, we chose 3 climate variables, including Ta, VPD, and SM, because they represent the fundamental heat and water supply (atmosphere and soil) conditions for vegetation growth. The relationships are calculated using all the monthly data in the growing season to take both annual and seasonal variations into consideration, for a total study period representing 66 months for LPDR-X, LPRM-X, LPRM-C2, LPRM-C2, and SMOSMAP-IB VODs, and 48 months for SMAP-DCA and MCCA-SMAP VOD products.

VOD correlations with Ta

We find overall negative correlations between Ta and NDVI anomalies in the arid and semiarid regions of China, especially in eastern Inner Mongolia (Fig. 3A). The above phenomena are also shown by LPDR-X (Fig. 3B), LPRM-X (Fig. 3C), LPRM-C2 (Fig. 3D), LPRM-C1 (Fig. 3E), and SMOSMAP-IB VOD (Fig. 3H), indicating general reductions in both vegetation greenness and canopy biomass under warmer conditions in those moisture-limited regions. In contrast, vegetation tends to grow stronger with increasing Ta in northeastern and northern China, indicated by significant positive correlations between NDVI/VODs and Ta anomalies (Fig. 3). It is worth noting that the correlations of NDVI with Ta share similar spatial distributions to those of X- and C-band VODs, contrasting with quite different patterns from those of L-band VODs (Fig. 3).

However, apparent differences in the correlations of VOD anomalies with Ta can be found from different VOD products. In detail, LPDR-X and LPRM-X VODs show different responses to varying Ta over most areas of southern China, indicated by mostly nonsignificant correlations for LPDR-X (Fig. 3B) vs. significantly negative correlations for LPRM-X (Fig. 3C). The 2 C-band VODs generally share synchronous variations with varying Ta across the entire study domain. However, the 3 L-band VODs show obviously divergent responses to changing Ta in northern China, where MCCA-SMAP VOD (Fig. 3G) exhibits significant positive correlations, and SMOSMAP-IB VOD (Fig. 3H) indicates significant negative correlations with Ta anomalies during the study period. Such divergent responses are mainly due to the different algorithms and different satellite records used for VOD retrieval (details are shown in Methods). Moreover, all 7 VODs show strong discrepancies in their responses to Ta in southern China. The 2 X-band products (LPDR-X and especially LPRM-X) show negative responses to Ta (Fig. 3B and C), while opposite responses are found in the 2 C-band and 3 L-band VOD products (Fig. 3D to H). These contrasting relationships suggest that important impacts contributed by the underlying retrieval algorithms, frequencies, and sensors in capturing the vegetation response to changing Ta.

VOD correlations with VPD

Unlike Ta, NDVI and the 7 VOD products exhibit quite different responses to VPD changes over China during the study period (Fig. 4). NDVI (Fig. 4A) and LPDR-X VOD (Fig. 4B) generally vary negatively with changing VPD, whereas LPDR-X VOD shows more significant negative correlations with VPD over more regions in China than NDVI does. The other X-band VOD product, LPRM-X, exhibits significant negative correlations with VPD anomalies over almost half of China, mainly distributed across the northern, southeastern, and southwestern regions, while showing positive responses to VPD over the other half of China (Fig. 4C). The 2 C-band VOD products (Fig. 4D and E) show overall negative responses to VPD anomalies spanning northern China, similar to NDVI and X-band VODs, but indicate strong positive correlations elsewhere. We also find that SMAP-DCA (Fig. 4F) and MCCA-SMAP (Fig. 4G) VODs share similar strong positive variations with VPD across the study domain, while the latter shows even stronger positive responses to VPD. In contrast, SMOSMAP-IB VOD (Fig. 4H) exhibits similar responses to VPD with LPRM-X VOD (Fig. 4C), showing negative correlations over northern and southwestern China, and positive correlations over the rest of China. The above results indicate apparent difference among SMOSMAP-IB with SMAP-DCA and MCCA-SMAP VOD products, which suggests potential impacts from the different retrieval algorithms on the L-band VOD performance.

VOD correlations with SM

Stronger differences were found in the responses of different VOD products to SM anomalies compared to their responses to Ta and VOD anomalies (Fig. 5). Here, the surface SM (0 to 7 cm) from ERA5-Land is used as an independent SM product to quantify how VODs respond to soil water stress. Specifically, NDVI (Fig. 5A) and LPDR-X VOD (Fig. 5B) are significantly and positively correlated with SM variations over most regions in the study domain. In contrast, LPRM-X VOD (Fig. 5B) shows significant negative correlations with SM anomalies over more than half of the study domain spanning from northeastern to southwestern regions, indicating discrepancies in VOD capabilities in capturing SM-related impacts on vegetation due to different retrieval algorithms. Again, the 2 C-band VOD products share similar responses to varying SM (Fig. 5D and E), though the LPRM-C1 VOD tends to be more negatively correlated with SM anomalies than LPRM-C2. However, for the 3 L-band VOD products, the SMAP-DCA (Fig. 5F) and MCCA-SMAP (Fig. 5G) VODs show mostly negative responses to SM over most regions, whereas SMOSMAP-IB VOD (Fig. 5H) exhibits negative correlations with SM only across northeastern, southeastern, and southwestern China.

In summary, most of the VOD products examined (except LPRM-X) show significantly positive responses to Ta changes across most of China (Fig. S2A), and the positive responses are stronger for VODs at lower frequencies. VOD correlations to VPD and SM changes are also higher with lower retrieval frequencies, but the relationships vary from negative (X-band) to positive (C- and L-band) with VPD (Fig. S3A). The opposite is true for SM (Fig. 6A). It should be noted that the results from the partial correlation analyses of VOD variations with Ta, VPD, and SM anomalies (Figs. S4 to S6) are quite similar to the results of correlations conducted separately for the above variables shown in Figs. 3 to 5 despite casual correlations among these variables, indicating that the above analyses on the VOD responses to Ta, VPD, and SM variations are robust. Thus, different VOD products retrieved from different algorithms, frequencies, and sensors show different capabilities in representing vegetation dynamics under a changing climate, which need to be carefully considered

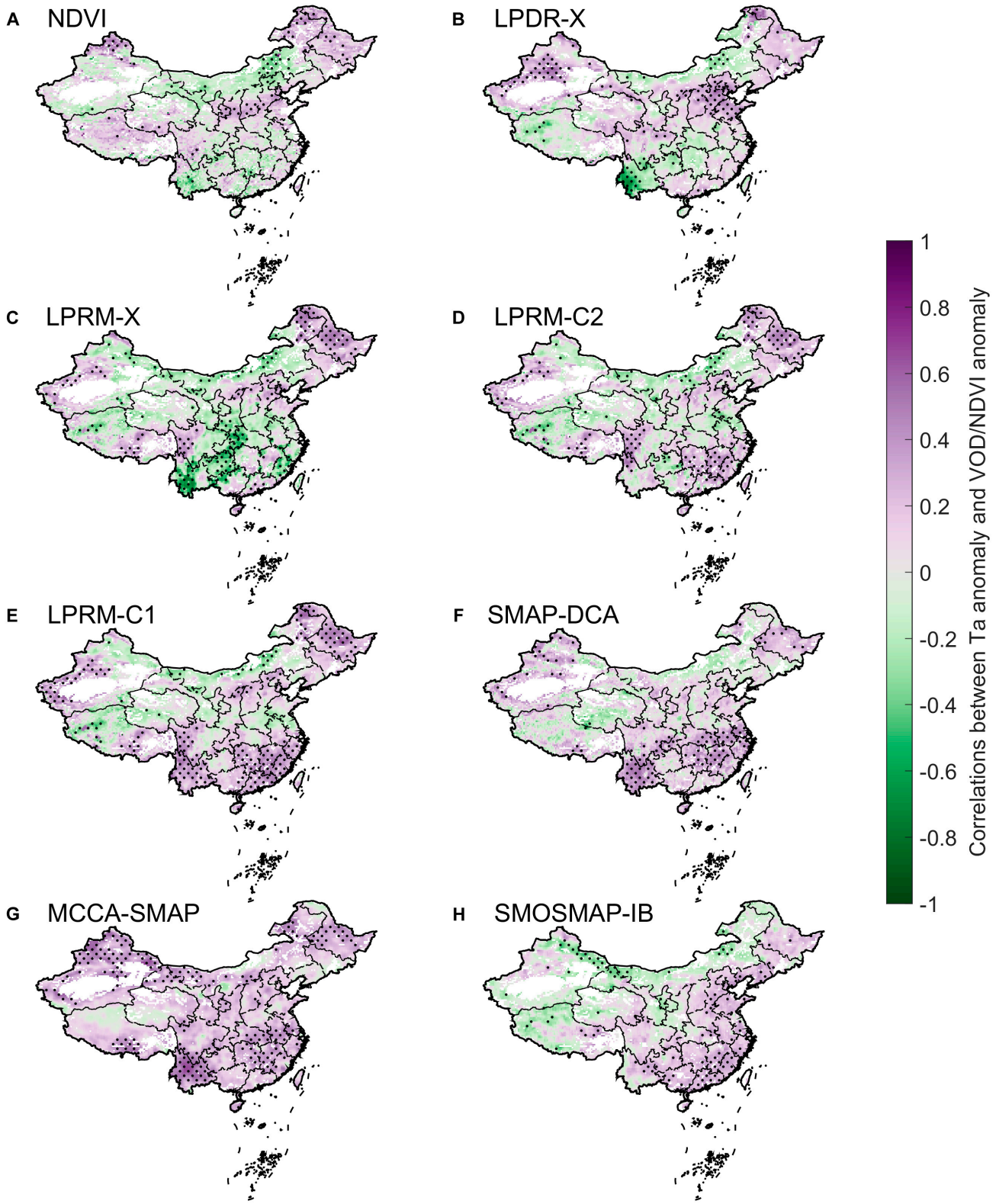

Fig. 3. Spatial patterns of the correlations between the growing-season Ta anomaly and VOD anomalies in China for 2012 to 2022. Correlations of the growing-season anomaly from MODIS NDVI (A), AMSR-E/AMSR2 LPDR X-band (LPDR-X; B), AMSR2 LPRM X-band (LPRM-X; C), AMSR2 LPRM C2-band (LPRM-C2; D), AMSR2 LPRM C1-band (LPRM-C1; E), SMAP operational L-band DCA product (SMAP-DCA; F), SMAP MCCA L-band (MCCA-SMAP; G), and SMOS/SMAP fused L-band VOD product (SMOSMAP-IB; H), with Ta anomaly are shown. Pixels with black dots indicate significant ($P < 0.05$) correlations. Note that the study period for SMAP-DCA and MCCA-SMAP VODs is from 2015 to 2022.

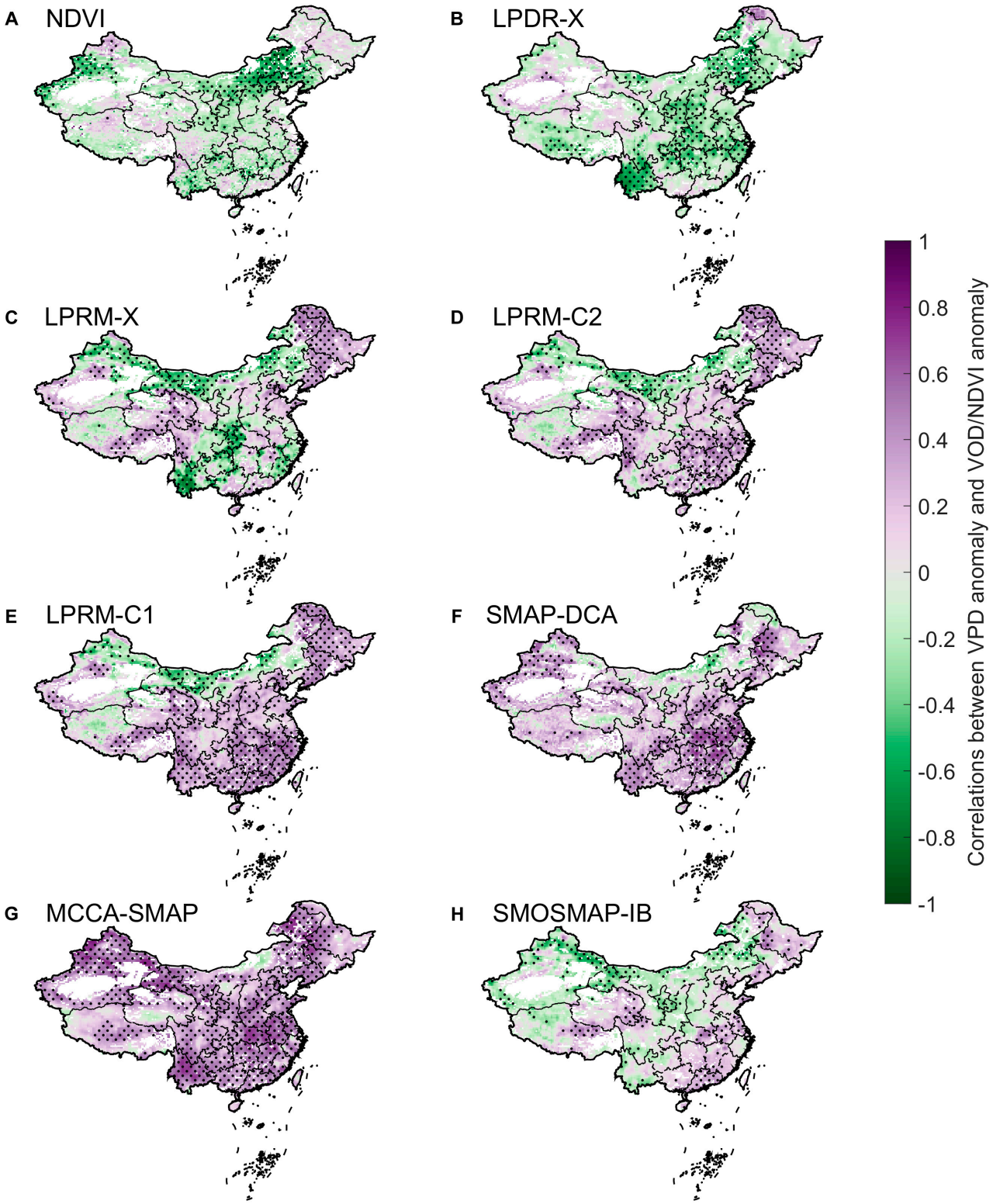

Fig. 4. Correlations between the growing-season VPD anomaly and VOD anomalies in China for 2012 to 2022. Correlations of the growing-season anomaly from MODIS NDVI (A), AMSR-E/AMSR2 LPDR X-band (LPDR-X; B), AMSR2 LPRM X-band (LPRM-X; C), AMSR2 LPRM C2-band (LPRM-C2; D), AMSR2 LPRM C1-band (LPRM-C1; E), SMAP operational L-band DCA product (SMAP-DCA; F), SMAP MCCA L-band (MCCA-SMAP; G), and SMOS/SMAP fused L-band VOD product (SMOSMAP-IB; H), with VPD anomaly are shown. Pixels with black dots indicate significant ($P < 0.05$) correlations. Correlations are estimated from 2012 to 2022, except for SMAP-DCA and MCCA-SMAP, for which correlations are calculated from 2015 to 2022.

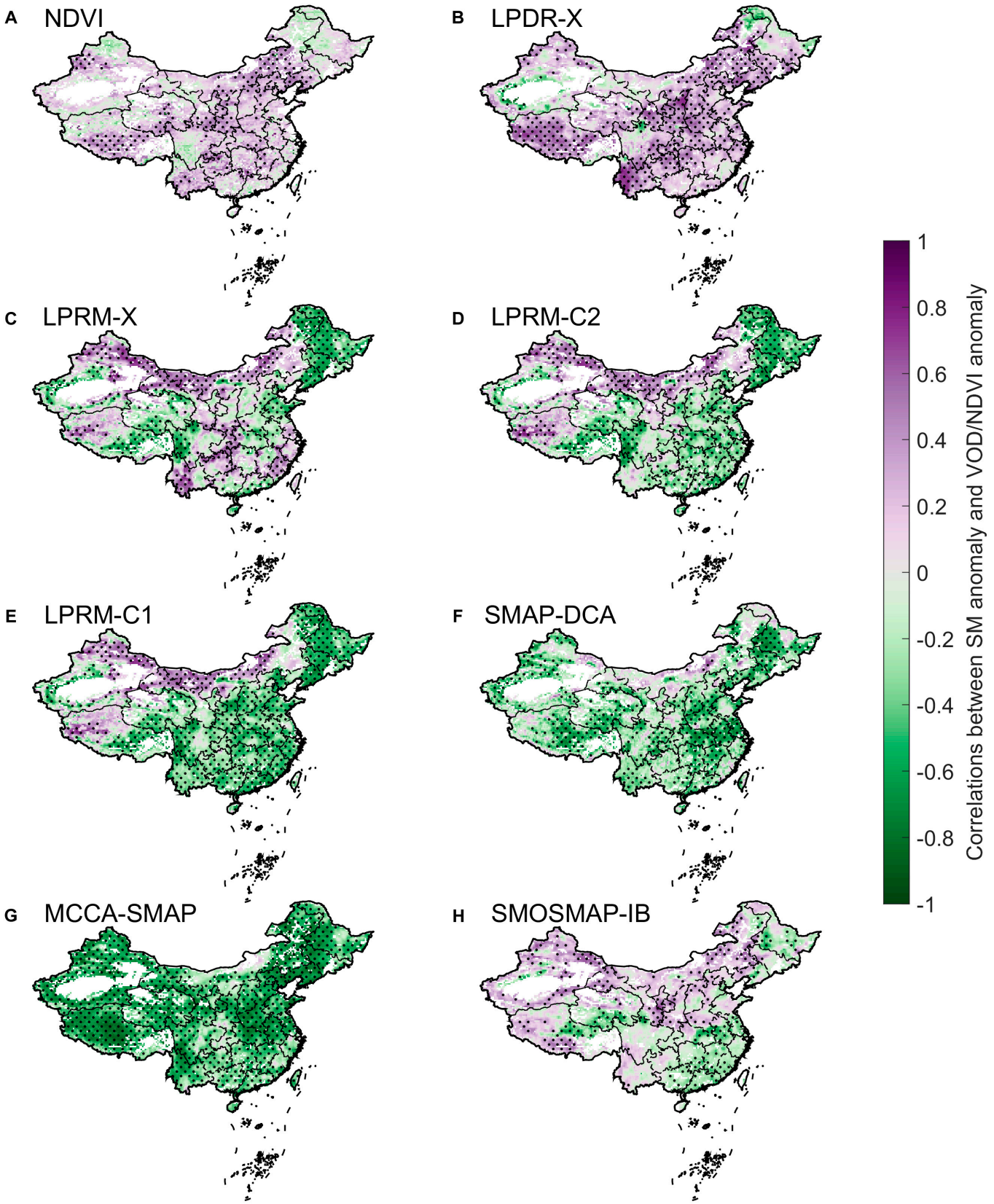

Fig. 5. Similar to Figs. 4 and 3, but for the correlations of the growing-season surface soil moisture (SM) anomaly with VOD anomalies for 2012 to 2022 in China. The SM is obtained from the ERA5-Land surface (0 to 7 cm) SM product. Correlations of the growing-season anomaly from MODIS NDVI (A), AMSR-E/AMSR2 LPDR X-band (LPDR-X; B), AMSR2 LPRM X-band (LPRM-X; C), AMSR2 LPRM C2-band (LPRM-C2; D), AMSR2 LPRM C1-band (LPRM-C1; E), SMAP operational L-band DCA product (SMAP-DCA; F), SMAP MCCA L-band (MCCA-SMAP; G), and SMOS/SMAP fused L-band VOD product (SMOSMAP-IB; H), with SM anomaly are shown. Pixels with black dots indicate significant ($P < 0.05$) correlations.

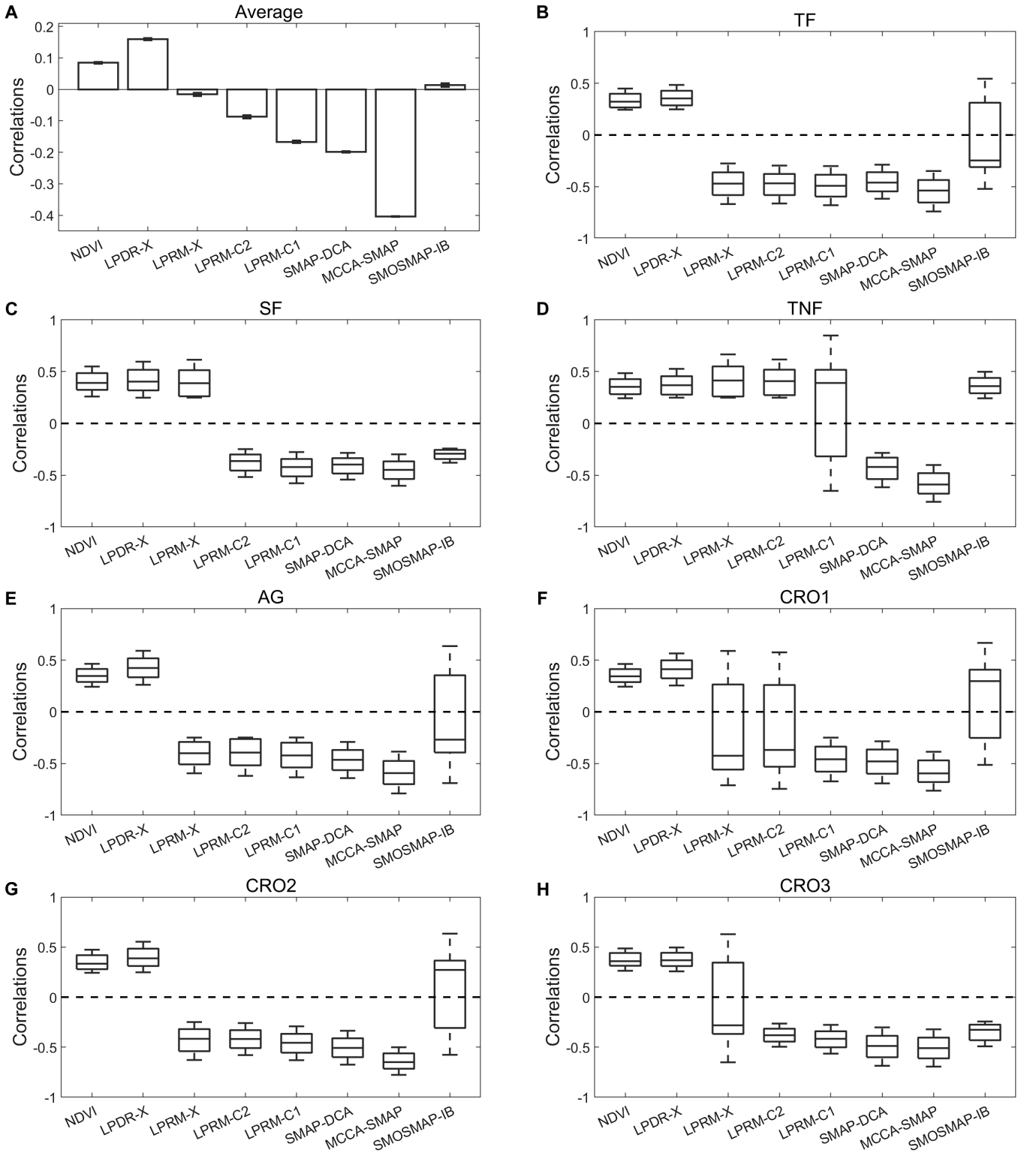

Fig. 6. Significant correlations of the growing-season SM anomaly with VOD anomaly across different PFTs in China. Only pixels with significant ($P < 0.05$) correlations are included here. The area-weighted correlations of SM anomalies with VOD anomalies spanning the entire China are shown in (A), with the error bars indicating the standard errors of the correlations for each PFT. Panels (B) to (H) indicate the significant ($P < 0.05$) correlations across each PFT. Note that the correlations for SMAP-DCA and MCCA-SMAP VODs are calculated for 2015 to 2022.

for optimal and wider applications. More importantly, the VODs show stronger responses to water stresses (VPD and SM) than to Ta changes, indicating stronger capabilities of VOD to capture vegetation dynamics under water stress than Ta limitations.

The responses of VOD to climate variations across different PFTs in China

The significant ($P < 0.05$) relationships between different VOD products and climate variables vary distinctively across different

vegetation types. As VOD products respond more closely to water stress than Ta, especially SM constraints, hereafter we focus our analyses on the VOD response to varying SM across different PFTs in China. Spanning the entire study domain, LPDR-X exhibits the highest positive correlations ($r = 0.16$, $P < 0.05$), while MCCA-SMAP shows the strongest negative responses to SM variations ($r = -0.40$, $P < 0.05$), suggesting that retrieval frequency has the strongest impacts on VOD variations, followed by the retrieval algorithms (Fig. 6A). Moreover, these VOD products generally vary with SM stresses following their retrieval frequencies across different PFTs, though differences exist (Fig. 6B to H). An exception is found in TNF (Fig. 6D), where NDVI, X- and C-band VODs, and SMOSMAP-IB VODs are positively correlated with changing SM. Water is a major limiting factor in TNF, and the canopy water stress could be well captured by X- and C-band VODs there, further emphasizing the impacts of different retrieval frequencies on VOD responses to SM variations. In addition, the responses of VODs to Ta and VPD variations over different PFTs in China are also found to vary generally with their retrieval frequencies and algorithms (Figs. S2 and S3, respectively).

Furthermore, VOD responses to changing Ta (Fig. S7), VPD (Fig. S8), and SM (Fig. 7) vary across different months and different PFTs in China. Generally, a shift from positive to negative responses to SM variations is generally observed in NDVI and VOD products retrieved from high to low frequencies across the entire growing season, except for TNF. For water-limited ecosystems such as the TNF, the correlation of NDVI and X- and C-band VODs to SM varies from slightly negative values in April (the beginning of the growing season) to positive in later months, achieving the strongest positive values at the peak of the growing season (Fig. 7C). However, the 3 L-band VODs exhibit similar correlation strength, but differing directional responses to SM throughout the growing season (negative for SMAP-DCA and MCCA-SMAP, and positive for SMOSMAP-IB), suggesting that the deeper penetration of the L-band signals may be less suitable for distinguishing the SM influence on VOD in the sparsely vegetated TNF. For other ecosystems, the VOD variations under varying SM show minimal seasonality during the growing season, as several factors may work together to drive vegetation dynamics over these PFTs. The above results are also true for the VOD responses to VPD (Fig. S8). However, for Ta, the exception is found in TF (Fig. S7A). VODs generally show strong increases at the beginning of the growing season, and such increases are weakened and even decline after the peak of the growing season in TF (Fig. S7A). X-band VODs initially exhibit significant declines with Ta warming, followed by the C-band VODs. However, the L-band VODs still increase (but only slightly) with increasing Ta after the peak of the growing season in TF, indicating more direct responses of the higher-frequency VODs than the lower ones to represent the Ta limitations on TF in China.

The carry-over effects of climate on vegetation dynamics

In order to assess whether VOD products have the ability to capture carry-over effects of climate variations on vegetation in China, here we show the relationships of Ta, VPD, and SM anomalies from both previous and current months with data from only the current month. Generally, Ta (Fig. S9) and VPD (Fig. S10) exert carry-over effects on vegetation dynamics indicated by stronger positive or negative VOD correlations with previous month environmental conditions than for results derived only using data from the current month for different PFTs. Moreover, the carry-over effects are more prevalent for vegetation responses to SM (Fig. 8). In particular, in TNF, where the ecosystems are generally water limited, VOD correlations with SM are largely improved when SM from the previous month is included (Fig. 8C). Moreover, VODs retrieved from higher frequencies (i.e., X-band) reveal stronger SM carry-over effects than from lower frequencies. For relatively humid forest ecosystems, such as TF (Fig. 8A) and SF (Fig. 8B), the SM carry-over effects on vegetation dynamics are relatively small, likely because these ecosystems are generally not water limited and trees have deep roots. Thus, there are carry-over effects of climate variation on vegetation dynamics in China, which should be carefully considered in climate change and ecosystem assessment studies.

Discussion

In this study, we find divergent responses of different VODs to climate variations across China, according to their retrieval frequencies, algorithms, and sensors. Because of relatively high retrieval frequencies, X-band (LPDR-X and LPRM-X) and C-band (LPRM-C1 and LPRM-C2) VODs are generally assumed to show direct (or immediate) variations from upper canopy under a varying climate, such as positive responses of X-band VOD to SM in TNF (Fig. 6C). However, microwave signals at lower frequencies can penetrate deeper into the canopy, and thus, L-band VOD can include greater sensitivity to the woody component of vegetation, and sometimes even understory vegetation [43]. Irrespective of the differences from retrieval algorithms, X- and C-band VODs generally show stronger seasonal variations than L-band VOD, further confirming that VOD products derived from high frequencies represent more dynamic upper canopy variations responsive to climate variability.

VOD was widely compared with many vegetation proxies, such as NDVI, AGB, tree height, and so on, to reveal its ability to detect vegetation status. L-band VOD was found to show advantages in capturing AGB variations [5,10]. Moreover, L-band VOD was also shown to have high correlations with tree height [43], a key parameter closely linked to AGB, further indicating its ability to capture AGB dynamics, which may explain the generally positive or nonsignificant correlations of Ta/VPD with SMAP-DCA and MCCA-SMAP VODs across most regions in China shown in this study (Fig. 3). Our results show that X-band VOD (Fig. 4C) has the highest advantages than the other VODs to successfully detect the impacts of atmospheric water stress on vegetation, which is consistent with previous studies [23,44].

The VOD variations responding to climate also vary across different PFTs, mainly attributed to different vegetation growth limitations. For example, in SF, where Ta is not the dominant limiting factor despite the prevalence of high temperature that may negatively impact vegetation growth, only X-band VOD products demonstrate negative effects of high Ta on VOD (Fig. 3C). The vegetation canopy responds quickly to warming and X-band VOD may have better capabilities to detect the above responses than other VODs. Moreover, X-band VOD products show significant negative responses to Ta (Fig. 3B and C) and VPD (Fig. 4B and C) increases, as well as positive responses to SM variations (Fig. 5B and C) in the regions with high Ta and low precipitation (Fig. S1), which are consistent with recent studies showing significant vegetation growth reductions under compound heatwave and drought events in China [45]. These results

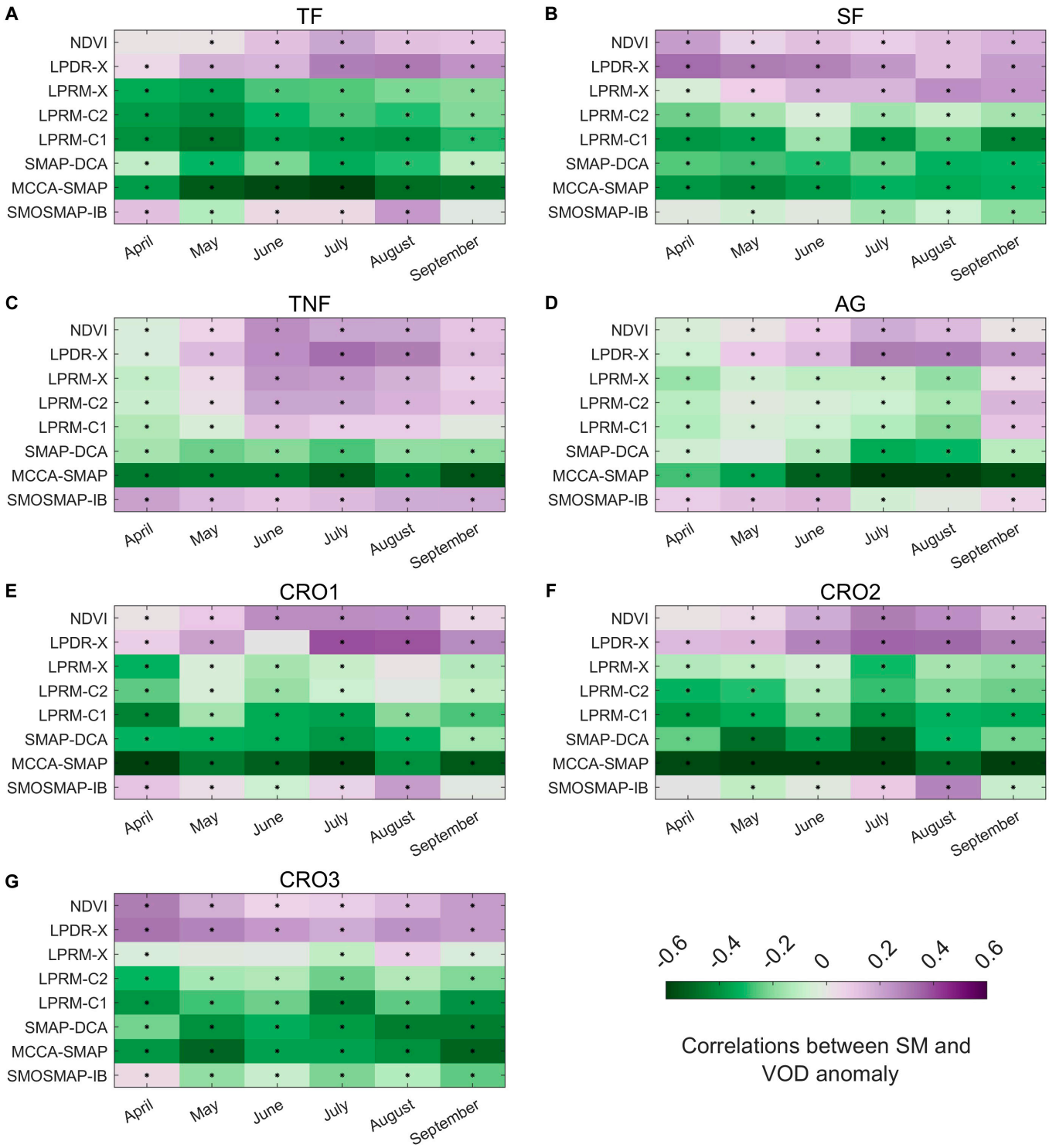

Fig. 7. Correlations of VODs with surface (0 to 7 cm) SM anomalies for different PFTs and growing-season months in China during the study period. Panels (A) to (G) indicate the correlations of VODs with SM anomalies across each PFT. The surface SM from ERA5-Land is used here. The significant correlations ($P < 0.05$) are marked with "*".

suggest that X-band VODs, especially LPRM-X VOD, have higher priority than the other VODs to be employed to investigate the impacts of heatwaves and drought on vegetation in these dry and hot regions. Furthermore, vegetation productivity was found to be positively correlated with VPD in some areas over the northern terrestrial ecosystems, where negative correlations between vegetation productivity and VPD were shown in most regions [46]. Therefore, LPRM-X and SMOSMAP-IB VODs potentially outperform the other VODs to represent vegetation responses to VPD variations over China (Fig. 4). In terms of vegetation responses to SM variations, previous studies showed that different vegetation types have different responses to SM variations, some of which may have water retention effects, while others have water consumption effects, showing positive

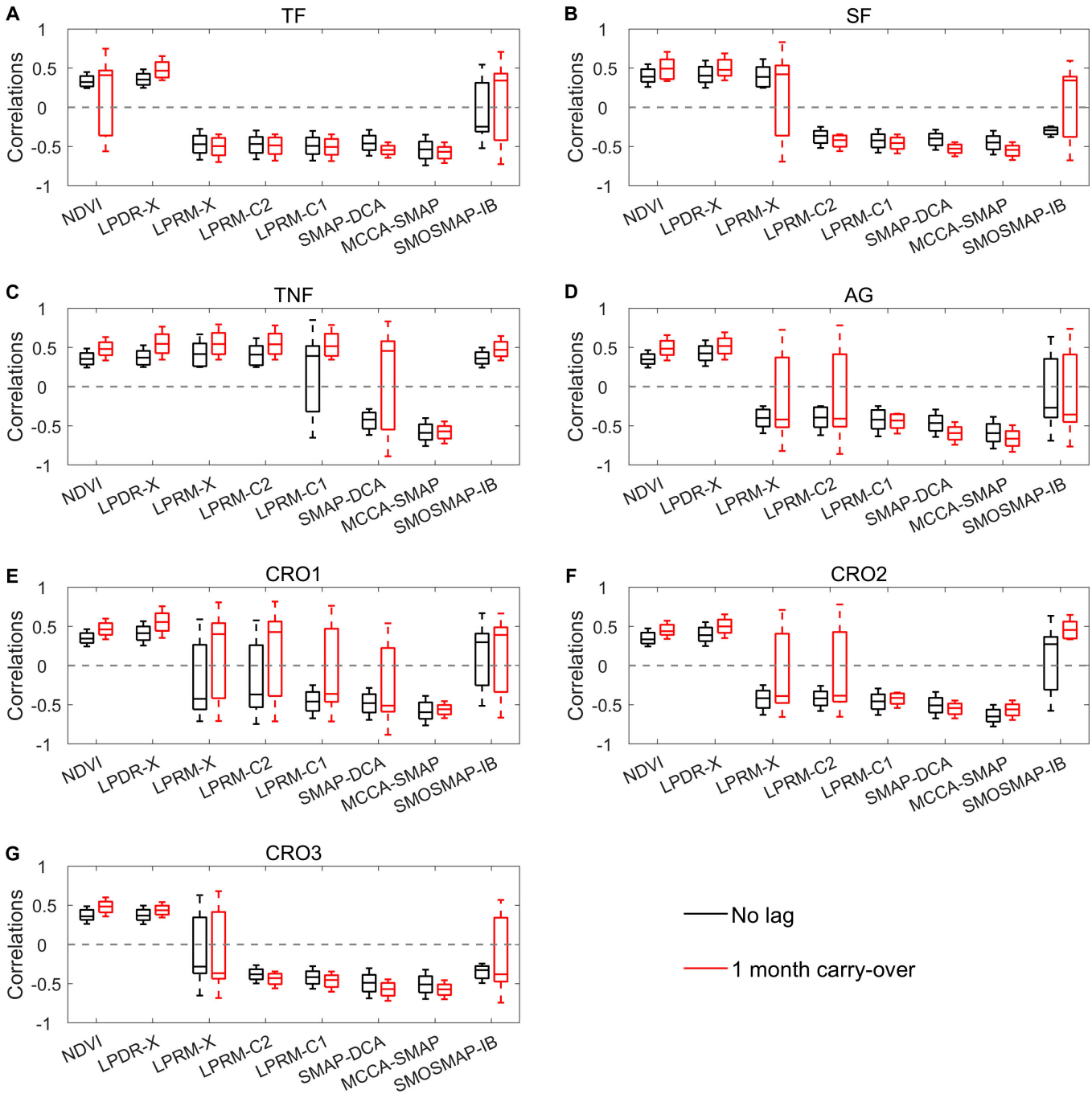

Fig. 8. Correlations of VOD anomalies with SM anomalies from only the current month (No lag) and with SM anomalies averaged from both previous and current months (1 month carry-over) during the growing season of 2012 to 2022 across different PFTs. Panels (A) to (G) indicate the correlations of VOD anomalies with SM anomalies from the current month (No lag) and with SM anomalies averaged from both previous and current months (1 month carry-over) across each PFT. Note that the study period for SMAP-DCA and MCCA-SMAP VODs is from 2015 to 2022.

and negative relationships across different ecosystems [47]. From this perspective, LPRM-X, LPRM-C2, and LPRM-C1, together with SMOSMAP-IB VODs, exhibit the most reasonable responses to SM variations among all the examined VODs (Fig. 5) over the study domain.

Vegetation was found to have carry-over effects from prior growing conditions influencing the present growth. Thus, the effects of climate variations on vegetation dynamics could persist from a previous state to current ones. Xia et al. [48] have shown that the effects of summer warming on plant growth and primary production carried over into other seasons. Late spring frost was stated to have more severe and long-lasting carry-over effects on forests than growing-season drought in the Northern Hemisphere [49]. The effects of previous temperature and moisture conditions on present vegetation growth were examined to reveal patterns of intrinsic and extrinsic strength and length of carry-over effects of Ta and SM on vegetation responses across global drylands [50]. Lian et al. [51] reported a carry-over effect of SM deficit during spring greening on vegetation responses to Ta in the subsequent summer.

In this study, we find significant 1-month carry-over effects of SM on vegetation dynamics (Fig. 8), consistent with the results in previous studies. Moreover, we find that the VODs well capture the 1-month carry-over effects of SM on vegetation in TNF, where water is a major limiting factor for vegetation growth. In particular, the SMAP-DCA VOD exhibits substantial carry-over effects, with associated VOD correlations with SM variations changing from negative to mostly positive values in TNF when including SM from the previous month (Fig. 8C). We also find carry-over effects of Ta and VPD on vegetation dynamics (Figs. S9 and S10), which have received relatively little attention in previous studies, and should be addressed in future research.

In order to further clarify the capabilities of VODs to detect vegetation water status changes, the corresponding SM of each VOD product is also included for comparisons with the results using ERA5-Land surface SM (0 to 7 cm) here (Fig. 9). Although the correlations using the corresponding satellite surface SM retrievals are slightly stronger than that from the ERA5-Land SM, the 3 L-band VODs show generally similar responses to SM no matter which SM data are used (Fig. 9E to H). This finding suggests that there are limited effects of the retrieval algorithms on the ability of L-band VOD responding to SM stress. Moreover, L-band microwave signals are more sensitive to surface SM variations and lead to more robust SM retrievals. However, substantial differences could be found for LPRM-X and LPRM-C2 VODs (Fig. 9H), where the SM relationships change from negative correlations using ERA5-Land to positive using the corresponding sensor-derived SM. LPRM-C1 (Fig. 9D) also correlates with its corresponding SM positively over more regions than with ERA5-Land SM, though this phenomenon is less obvious than LPRM-X and LPRM-C2. While direct validations of large-scale VOD products remain challenging, the associated SM retrievals have been widely evaluated recently, including the C- and X-band LPRM retrievals from AMSR-E and AMSR-2, and L-band retrievals from SMAP and SMOS [52–54]. The above studies generally showed reasonable performance of the SM products especially for L-band retrievals. Therefore, the performance of different VOD products could be indirectly evaluated through the above comparisons of VOD correlations with ERA5-Land SM product and the corresponding SM retrievals. Moreover, those results further suggest that the retrieval frequency is the most critical factor for VOD capabilities to identify vegetation responses to SM stress in China. The VODs from different frequencies, algorithms, and sensors may also offer potentially complimentary information about vegetation dynamics at different canopy levels. Asynchronous variations in different VODs could reveal important information in vegetation phenology, growth, and water status between foliar and woody biomass components that influence vegetation dynamics under different climate conditions [55]. Thus, comprehensive assessments should be carefully taken for choosing the appropriate VOD products as vegetation proxies for any regional applications.

It should be noted that there are some limitations in this study. The accuracy of VOD retrievals is affected by radio frequency interference (RFI), the microwave signals emitted by artificial devices and received by satellite sensors, which varies with sensor, frequency, and location. Data from SMOS is more influenced by RFI in China, resulting in significant data loss or retrieval errors [56,57]. Such RFI limitations on SMOS data are propagated to SMOSMAP-IB VOD and SM data; however, such issues could be partly compensated by fusing with SMAP data, which is equipped by improved RFI filtering methods [5]. This may partly explain the differences in the performance between SMOSMAP-IB and the 2 other SMAP-based VOD products. SMAP-DCA utilizes MODIS NDVI as ancillary data in its VOD retrievals, whereas MCCA-SMAP and SMOSMAP-IB do not incorporate any ancillary vegetation information in data production, which may also contribute to differences in those L-band VODs. Field measurements of biomass, leaf area index, leaf water potential, and vegetation structure could be further conducted to better understand the variations of VOD at different frequencies [58]. Another limitation of this study is that the analyses of these VOD products are based on different time periods (Fig. S11). We investigate VOD responses to Ta, VPD, and SM across China from 2012 to 2022 for LPDR-X, LPRM-X, LPRM-C1, LPRM-C2, and SMOSMAP VODs, in comparison with that from 2015 to 2022 for SMAP-DCA and MCCA-SMAP VODs, which may contribute uncertainties in the results (Fig. S11). Distinct VOD responses to Ta, VPD, and SM are shown for croplands, likely due to different management practices, regions, and planted crop types, requiring further analyses to identify the capabilities of different VODs to track crop dynamics in China. This study chooses the period from April to September as the growing season for the investigations, which may introduce some uncertainties in the results, as vegetation located in the northern part of China or Tibetan Plateau may not start to grow in April. However, the growing season for most vegetation over China is April to September, and thus, we consider April to September as the growing season to conduct the analyses in this study. In addition, the ability of VOD to represent vegetation dynamics under extremely high Ta and VPD or low SM conditions is not fully addressed in this study, limiting potential applications under more extreme climate conditions. Moreover, the interactions between any 2 climate factors may have distinct impacts on vegetation growth and hence VOD performance during the study period, which are also not considered here. Further studies are needed to evaluate the compounding effects from Ta, VPD, and SM stresses on VOD performance in China, as well as effects of compound climate extreme events. Finally, the SM datasets used in this study show limited ability to capture the influence of irrigation in croplands, particularly affecting result interpretation in areas with significant paddy rice, such as in Hunan and Jiangxi provinces. An improved SM dataset to adequately represent the irrigation effects on VOD variations is urgently needed. Additionally, we use surface SM in this study to investigate the VOD responses to soil water stress. However, surface SM is dynamic and may not be representative for some PFTs, such as TF and SF, which have deep roots. Root-zone SM should be incorporated in future studies to overcome this limitation.

Conclusion

In this study, we evaluate the capabilities of 7 VOD products to detect vegetation responses to climate variations from 2012 to 2022 (2015 to 2022 for SMAP-DCA and MCCA-SMAP) in China. Although they share similar spatial patterns, all 7 VODs exhibit divergent responses to climate variations in China, mainly varying with their retrieval frequencies, and followed by the retrieval algorithms and sensors. However, we also find consistent VOD responses to climate in the ecosystems dominated by either temperature or water, such as temperate forests

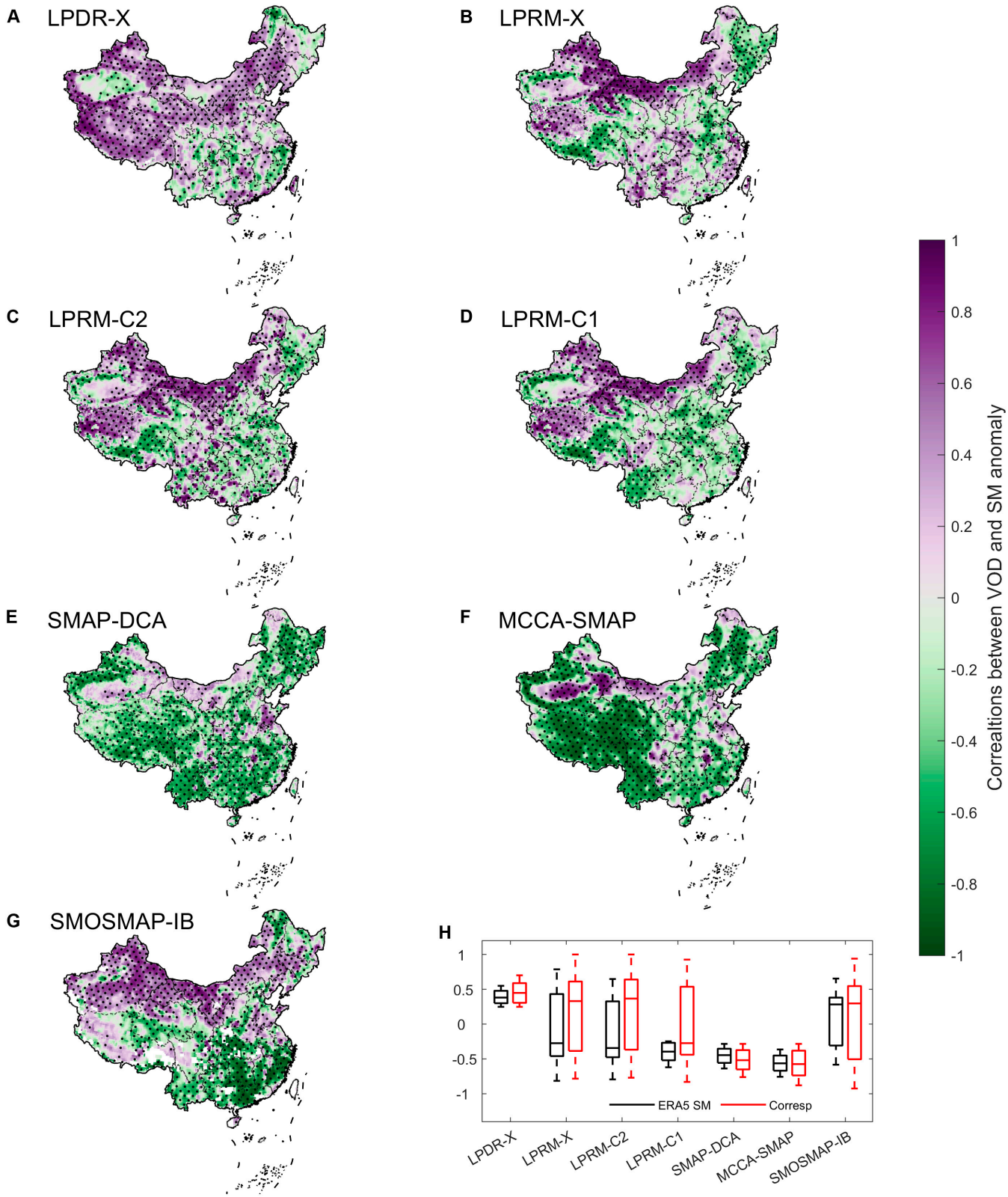

Fig. 9. Spatial distributions of the correlations between the growing-season VOD anomalies and the corresponding SM anomaly from 2012 to 2022 in China. The surface SM retrievals accompanying each VOD product were shown here, including LPDR-X (A), LPRM-X (B), LPRM-C2 (C), LPRM-C1 (D), SMAP-DCA (E), MCCA-SMAP (F) and SMOSMAP-IB (G). Comparisons between the correlations of using ERA5-Land SM product (ERA5 SM) and the corresponding SM (Corresp) of each VOD product are shown in panel (H). Pixels with black dots indicate significant ($P < 0.05$) correlations. Note that the study period for SMAP-DCA and MCCA-SMAP VODs is from 2015 to 2022.

(temperature-limited) and temperate grasslands and shrublands (water-limited). Furthermore, X- and C-band VODs show relatively higher potential to capture the carry-over effects of climate on vegetation dynamics than L-band VODs, as they mainly represent vegetation upper canopy dynamics, especially in arid and semiarid ecosystems. Our results highlight that the retrieval frequency is the most critical factor influencing VOD-based vegetation responses to changing climate in China, followed by the nature of the underlying retrieval algorithms and sensors. Thus, our results underscore that VOD products from different retrieval frequencies, algorithms, and sensors should be carefully evaluated for the study domain to select the most appropriate or complimentary VOD products for regional ecosystem studies, and to improve understanding of how vegetation dynamics are responding to the changing climate in China.

Acknowledgments

Funding: The work was supported by the National Natural Science Foundation of China (Grant nos. 42371355 and 42471114), the International Science and Technology Cooperation Program under the 2023 Shanghai Action Plan for Science, Technology and Innovation (Grant no. 23230712800), and "the Fundamental Research Funds for the Central Universities". R.R. was supported by the SMAP mission.

Author contributions: M.H.: Conceptualization, methodology, writing—original draft, and software. Y.Y.: Conceptualization and writing—review and editing. X.L.: Writing—review and editing, and data curation. J.-P.W.: Writing—review and editing, and data curation. J.S.K.: Writing—review and editing. R.R.: Writing—review and editing. L.F.: Writing—review and editing. H.W.C.: Writing—review and editing.

Competing interests: The authors declare that they have no competing interests.

Data Availability

AMSR2 VOD products, including X-, C1-, and C2-band data, can be downloaded from https://disc.gsfc.nasa.gov/datasets/. The AMSR LPDR X-band VOD product can be obtained from the Numerical Terradynamic Simulation Group (NTSG) website (http://files.ntsg.umt.edu/data/LPDR_v3/). The SMAP operational L-band DCA VOD products are available from https://nsidc.org/data/spl3smp_e/versions/6. The MCCA-SMAP VOD products are freely available from https://data.tpdc.ac.cn/en/data/034b78c9-80d1-47f1-9e19-eeaf2a309010/. The SMOSMAP-IB VOD products are available on the INRAE Bordeaux remote sensing products website (https://ib.remote-sensing.inrae.fr/).

Supplementary Materials

Figs. S1 to S11

References

1. Cui T, Fan L, Ciais P, Fensholt R, Frappart F, Sitch S, Chave J, Chang Z, Li X, Wang M, et al. First assessment of optical and microwave remotely sensed vegetation proxies in monitoring aboveground carbon in tropical Asia. *Remote Sens Environ*. 2023;293:Article 113619.
2. Forkel M, Schmidt L, Zotta R-M, Dorigo W, Yebra M. Estimating leaf moisture content at global scale from passive microwave satellite observations of vegetation optical depth. *Hydrol Earth Syst Sci*. 2023;27(1):39–68.
3. Peng Z, Zhao T, Shi J, Hu L, Rodríguez-Fernández NJ, Wigneron J-P, Jackson TJ, Walker JP, Cosh MH, Yang K, et al. First mapping of polarization-dependent vegetation optical depth and soil moisture from SMAP L-band radiometry. *Remote Sens Environ*. 2024;302:Article 113970.
4. Chang Z, Fan L, Wigneron J-P, Wang Y-P, Ciais P, Chave J, Fensholt R, Chen JM, Yuan W, Ju W, et al. Estimating aboveground carbon dynamic of China using optical and microwave remote-sensing datasets from 2013 to 2019. *J Remote Sens*. 2023;3:5.
5. Li X, Wigneron J-P, Frappart F, Fan L, Ciais P, Fensholt R, Entekhabi D, Brandt M, Konings AG, Liu X, et al. Global-scale assessment and inter-comparison of recently developed/reprocessed microwave satellite vegetation optical depth products. *Remote Sens Environ*. 2021;253:Article 112208.
6. Du J, Kimball JS, Sheffield J, Velicogna I, Zhao M, Pan M, Fisher CK, Beck HE, Watts JD, A G, et al. Synergistic satellite assessment of global vegetation health in relation to ENSO-induced droughts and pluvials. *J Geophys Res Biogeosci*. 2021;126(5):Article e2020JG006006.
7. Zhang Y, Zhou S, Gentine P, Xiao X. Can vegetation optical depth reflect changes in leaf water potential during soil moisture dry-down events? *Remote Sens Environ*. 2019;234:Article 111451.
8. Rao K, Anderegg WRL, Sala A, Martínez-Vilalta J, Konings AG. Satellite-based vegetation optical depth as an indicator of drought-driven tree mortality. *Remote Sens Environ*. 2019;227:125–136.
9. Jones MO, Jones LA, Kimball JS, McDonald KC. Satellite passive microwave remote sensing for monitoring global land surface phenology. *Remote Sens Environ*. 2011;115(4):1102–1114.
10. Wigneron J-P, Fan L, Ciais P, Bastos A, Brandt M, Chave J, Saatchi S, Baccini A, Fensholt R. Tropical forests did not recover from the strong 2015–2016 El Niño event. *Sci Adv*. 2020;6(6):eaay4603.
11. Fan L, Dong G, Frappart F, Wigneron J-P, Yue Y, Xiao X, Zhang Y, Tao S, Cao L, Li Y, et al. Satellite-observed increase in aboveground carbon over Southwest China during 2013-2021. *J Remote Sens*. 2024;4:113.
12. Fan L, Wigneron J-P, Ciais P, Chave J, Brandt M, Fensholt R, Saatchi SS, Bastos A, Al-Yaari A, Hufkens K, et al. Satellite-observed pantropical carbon dynamics. *Nat Plants*. 2019;5:944–951.
13. Wigneron J-P, Ciais P, Li X, Brandt M, Canadell JG, Tian F, Wang H, Bastos A, Fan L, Gatica G, et al. Global carbon balance of the forest: Satellite-based L-VOD results over the last decade. *Front Remote Sens*. 2024;5: 10.3389/frsen.2024.1338618.
14. Tong X, Brandt M, Yue Y, Ciais P, Rudbeck Jepsen M, Penuelas J, Wigneron J-P, Xiao X, Song X-P, Horion S, et al. Forest management in southern China generates short term extensive carbon sequestration. *Nat Commun*. 2020;11:129.
15. Fan L, Wigneron J-P, Ciais P, Chave J, Brandt M, Sitch S, Yue C, Bastos A, Li X, Qin Y, et al. Siberian carbon sink reduced by forest disturbances. *Nat Geosci*. 2023;16:56–62.
16. Yang H, Ciais P, Frappart F, Li X, Brandt M, Fensholt R, Fan L, Saatchi S, Besnard S, Deng Z, et al. Global increase in biomass carbon stock dominated by growth of northern young forests over past decade. *Nat Geosci*. 2023;16:886–892.
17. Teubner IE, Forkel M, Camps-Valls G, Jung M, Miralles DG, Tramontana G, van der Schalie R, Vreugdenhil M, Mösinger L, Dorigo WA. A carbon sink-driven approach to estimate gross

primary production from microwave satellite observations. *Remote Sens Environ*. 2019;229:100–113.
18. Wild B, Teubner I, Moesinger L, Zotta R-M, Forkel M, van der Schalie R, Sitch S, Dorigo W. VODCA2GPP—A new, global, long-term (1988–2020) gross primary production dataset from microwave remote sensing. *Earth Syst Sci Data*. 2022;14(3):1063–1085.
19. Moesinger L, Dorigo W, de Jeu R, van der Schalie R, Scanlon T, Teubner I, Forkel M. The global long-term microwave vegetation optical depth climate archive (VODCA). *Earth Syst Sci Data*. 2020;12(1):177–196.
20. Feldman AF, Short Gianotti DJ, Trigo IF, Salvucci GD, Entekhabi D. Land-atmosphere drivers of landscape-scale plant water content loss. *Geophys Res Lett*. 2020;47(22):Article e2020GL090331.
21. Konings AG, Piles M, Das N, Entekhabi D. L-band vegetation optical depth and effective scattering albedo estimation from SMAP. *Remote Sens Environ*. 2017;198:460–470.
22. Konings AG, Gentine P. Global variations in ecosystem-scale isohydricity. *Glob Change Biol*. 2017;23(2):891–905.
23. Li Y, Guan K, Gentine P, Konings AG, Meinzer FC, Kimball JS, Xu X, Anderegg WRL, McDowell NG, Martinez-Vilalta J, et al. Estimating global ecosystem isohydry/anisohydry using active and passive microwave satellite data. *J Geophys Res Biogeosci*. 2017;122(12):3306–3321.
24. Konings AG, Holtzman N, Rao K, Xu L, Saatchi SS. Interannual variations of vegetation optical depth are due to both water stress and biomass changes. *Geophys Res Lett*. 2021;48(16):Article e2021GL095267.
25. Schmidt L, Forkel M, Zotta R-M, Scherrer S, Dorigo WA, Kuhn-Régnier A, van der Schalie R, Yebra M. Assessing the sensitivity of multi-frequency passive microwave vegetation optical depth to vegetation properties. *Biogeosciences*. 2023;20(5):1027–1046.
26. Zhu Z, Piao S, Myneni RB, Huang M, Zeng Z, Canadell JG, Ciais P, Sitch S, Friedlingstein P, Arneth A, et al. Greening of the earth and its drivers. *Nat Clim Change*. 2016;6:791–795.
27. Li X, Wang K, Huntingford C, Zhu Z, Peñuelas J, Myneni RB, Piao S. Vegetation greenness in 2023. *Nat Rev Earth Environ*. 2024;5:241–243.
28. Chen C, Park T, Wang X, Piao S, Xu B, Chaturvedi RK, Fuchs R, Brovkin V, Ciais P, Fensholt R, et al. China and India lead in greening of the world through land-use management. *Nat Sustain*. 2019;2:122–129.
29. Du J, Kimball JS, Jones LA, Kim Y, Glassy J, Watts JD. A global satellite environmental data record derived from AMSR-E and AMSR2 microwave earth observations. *Earth Syst Sci Data*. 2017;9(2):791–808.
30. Du J, Kimball JS. Daily Global Land Parameters Derived from AMSR-E and AMSR2, Version 3 [data set], 2021; https://doi.org/https://doi.org/10.5067/WPXUQ72A4484
31. de Jeu R, Owe M. AMSR2/GCOM-W1 surface soil moisture (LPRM) L3 1 day 25 km x 25 km descending V001, edited by Goddard Earth Sciences Data and Information Services Center (GES DISC) (Bill Teng). Greenbelt (MD): Goddard Earth Sciences Data and Information Services Cente; 2014. https://doi.org/10.5067/CGDEOBASZ178
32. Owe M, de Jeu R, Holmes T. Multisensor historical climatology of satellite-derived global land surface moisture. *J Geophys Res Earth Surf*. 2008;113(F1):Article F01002.
33. Chaubell MJ, Yueh SH, Dunbar RS, Colliander A, Chen F, Chan SK, Entekhabi D, Bindlish R, O'Neill PE, Asanuma J, et al. Improved SMAP dual-channel algorithm for the retrieval of soil moisture. *IEEE Trans Geosci Remote Sens*. 2020;58(6):3894–3905.
34. O'Neill PE, Chan S, Njoku EG, Jackson T, Bindlish R, Chaubell J. *SMAP enhanced L3 radiometer global and polar grid daily 9 km EASE-grid soil moisture, version 5*. Boulder (CO): NASA National Snow and Ice Data Center Distributed Active Archive Center; 2021.
35. Zhao T, Shi J, Entekhabi D, Jackson TJ, Hu L, Peng Z, Yao P, Li S, Kang CS. Retrievals of soil moisture and vegetation optical depth using a multi-channel collaborative algorithm. *Remote Sens Environ*. 2021;257:Article 112321.
36. Li X, Wigneron J-P, Frappart F, De Lannoy G, Fan L, Zhao T, Gao L, Tao S, Ma H, Peng Z, et al. The first global soil moisture and vegetation optical depth product retrieved from fused SMOS and SMAP L-band observations. *Remote Sens Environ*. 2022;282:Article 113272.
37. Hu L, Zhao T, Ju W, Peng Z, Shi J, Rodríguez-Fernández NJ, Wigneron J-P, Cosh MH, Yang K, Lu H, et al. A twenty-year dataset of soil moisture and vegetation optical depth from AMSR-E/2 measurements using the multi-channel collaborative algorithm. *Remote Sens Environ*. 2023;292:Article 113595.
38. Peng Z, Zhao T, Yao P, Shi J. *SMAP soil moisture and vegetation optical depth product (9KM) using MCCA (2015-2023)*, National Tibet Plateau/Third Pole Environ Data Center; 2023.
39. Hersbach H, Bell B, Berrisford P, Hirahara S, Horányi A, Muñoz-Sabater J, Nicolas J, Peubey C, Radu R, Schepers D, et al. The ERA5 global reanalysis. *Q J R Meteorol Soc*. 2020;146(730):1999–2049.
40. Harris I, Osborn TJ, Jones P, Lister D. Version 4 of the CRU TS monthly high-resolution gridded multivariate climate dataset. *Sci Data*. 2020;7(1):109.
41. Friedl M, Sulla-Menashe D. MCD12Q1 MODIS/Terra+aqua land cover type yearly L3 global 500m SIN grid V006 [data set]. NASA EOSDIS L Process Distrib Act Arch Cent. 2019.
42. Orth R, Seneviratne SI. Analysis of soil moisture memory from observations in Europe. *J Geophys Res Atmos*. 2012;117(D15):Article D15115.
43. Rodríguez-Fernández NJ, Mialon A, Mermoz S, Bouvet A, Richaume P, Al Bitar A, Al-Yaari A, Brandt M, Kaminski T, Le Toan T, et al. An evaluation of SMOS L-band vegetation optical depth (L-VOD) data sets: High sensitivity of L-VOD to above-ground biomass in Africa. *Biogeosciences*. 2018;15(14):4627–4645.
44. Konings AG, Williams AP, Gentine P. Sensitivity of grassland productivity to aridity controlled by stomatal and xylem regulation. *Nat Geosci*. 2017;10:284–288.
45. Xu W, Yuan W, Wu D, Zhang Y, Shen R, Xia X, Ciais P, Liu J. Impacts of record-breaking compound heatwave and drought events in 2022 China on vegetation growth. *Agric For Meteorol*. 2024;344:Article 109799.
46. Zhong Z, He B, Wang Y-P, Chen HW, Chen D, Fu YH, Chen Y, Guo L, Deng Y, Huang L, et al. Disentangling the effects of vapor pressure deficit on northern terrestrial vegetation productivity. *Sci Adv*. 2023;9(32):eadf3166.
47. Peng C, Zeng J, Chen K-S, Li Z, Ma H, Zhang X, Shi P, Wang T, Yi L, Bi H. Global spatiotemporal trend of satellite-based soil moisture and its influencing factors in the early 21st century. *Remote Sens Environ*. 2023;291:Article 113569.
48. Xia J, Chen J, Piao S, Ciais P, Luo Y, Wan S. Terrestrial carbon cycle affected by non-uniform climate warming. *Nat Geosci*. 2014;7:173–180.

49. Chen L, Keski-Saari S, Kontunen-Soppela S, Zhu X, Zhou X, Hänninen H, Pumpanen J, Mola-Yudego B, Wu D, Berninger F. Immediate and carry-over effects of late-spring frost and growing season drought on forest gross primary productivity capacity in the northern hemisphere. *Glob Change Biol*. 2023;29(14):3924–3940.
50. Kusch E, Davy R, Seddon AWR. Vegetation-memory effects and their association with vegetation resilience in global drylands. *J Ecol*. 2022;110(7):1561–1574.
51. Lian X, Jeong S, Park C-E, Xu H, Li LZX, Wang T, Gentine P, Peñuelas J, Piao S. Biophysical impacts of northern vegetation changes on seasonal warming patterns. *Nat Commun*. 2022;13:3925.
52. Fan L, Xing Z, De Lannoy G, Frappart F, Peng J, Zeng J, Li X, Yang K, Zhao T, Shi J, et al. Evaluation of satellite and reanalysis estimates of surface and root-zone soil moisture in croplands of Jiangsu Province, China. *Remote Sens Environ*. 2022;282:Article 113283.
53. Wang P, Zeng J, Chen K-S, Ma H, Zhang X, Shi P, Peng C, Bi H. Global-scale assessment of multiple recently developed/reprocessed remotely sensed soil moisture datasets. *IEEE Trans Geosci Remote Sens*. 2024;62:1–18.
54. Fan X, Lu Y, Liu Y, Li T, Xun S, Zhao X. Validation of multiple soil moisture products over an intensive agricultural region: Overall accuracy and diverse responses to precipitation and irrigation events. *Remote Sens*. 2022;14(14):3339.
55. Wang X, Dannenberg MP, Yan D, Jones MO, Kimball JS, Moore DJP, van Leeuwen WJD, Didan K, Smith WK. Globally consistent patterns of asynchrony in vegetation phenology derived from optical, microwave, and fluorescence satellite data. *J Geophys Res Biogeosci*. 2020;125(7):Article e2020JG005732.
56. Al-Yaari A, Wigneron J-P, Dorigo W, Colliander A, Pellarin T, Hahn S, Mialon A, Richaume P, Fernandez-Moran R, Fan L, et al. Assessment and inter-comparison of recently developed/reprocessed microwave satellite soil moisture products using ISMN ground-based measurements. *Remote Sens Environ*. 2019;224:289–303.
57. Oliva R, Daganzo E, Kerr YH, Mecklenburg S, Nieto S, Richaume P, Gruhier C. SMOS radio frequency interference scenario: Status and actions taken to improve the RFI environment in the 1400–1427-MHz passive band. *IEEE Trans Geosci Remote Sens*. 2012;50(5):1427–1439.
58. Frappart F, Wigneron J-P, Li X, Liu X, Al-Yaari A, Fan L, Wang M, Moisy C, Le Masson E, Aoulad Lafkih Z, et al. Global monitoring of the vegetation dynamics from the vegetation optical depth (VOD): A review. *Remote Sens*. 2020;12(18):2915.

Journal of Remote Sensing
A SCIENCE PARTNER JOURNAL

Divergent Responses of Multi-frequency Vegetation Optical Depth Products to Climate Variations in China

Mingzhu He, Yonghong Yi, Xiaojun Li, Jean-Pierre Wigneron, John S. Kimball, Rolf Reichle, Lei Fan, and Hans W. Chen

Citation: He M, Yi Y, Li X, Wigneron J, Kimball J, Reichle R, Fan L, Chen H. Divergent Responses of Multi-frequency Vegetation Optical Depth Products to Climate Variations in China. *J Remote Sens*. 2026;**6**:1028. DOI: 10.34133/remotesensing.1028

Vegetation optical depth (VOD) has been widely assessed for satellite monitoring of vegetation carbon and water status under different environmental conditions. However, abilities of multi-frequency VODs to reflect the integrated dynamics in vegetation status under changing climate are still underinvestigated, especially in China, which has experienced substantial vegetation greening since 2000. To fill this gap, this study examines 7 VOD products for their capabilities to detect vegetation status changes under climate variations from 2012 to 2022 in China. We find divergent responses of multi-frequency VODs to climate variations in China, and the retrieval frequency is the most important factor, followed by the underlying retrieval algorithms. All 7 VOD products show stronger responses to water limitations (atmospheric and soil water stress) than temperature across different plant functional types in China, suggesting high potential of VOD to track vegetation water status changes. We also find that the capabilities of VODs to represent vegetation responses to climate variations are affected by vegetation growth limitations, showing consistent responses for ecosystems dominated by either temperature or water. Most importantly, we find that VODs capture well the carry-over effects of climate on vegetation dynamics in China, with X- and C-band VODs showing stronger abilities than L-band VODs, especially for ecosystems located in China's arid and semiarid regions. These findings address the divergent capabilities of multi-frequency VOD products to capture the vegetation responses to climate variations across China, promoting ecological applications of different VOD products in regional studies.
Image

Journal of Remote Sensing (ISSN 2694-1589) is published by the American Association for the Advancement of Science. 1200 New York Avenue NW, Washington, DC 20005.